Volume 149
Number 24
21 December 2024
Pages 5731-5916

Analyst

rsc.li/analyst

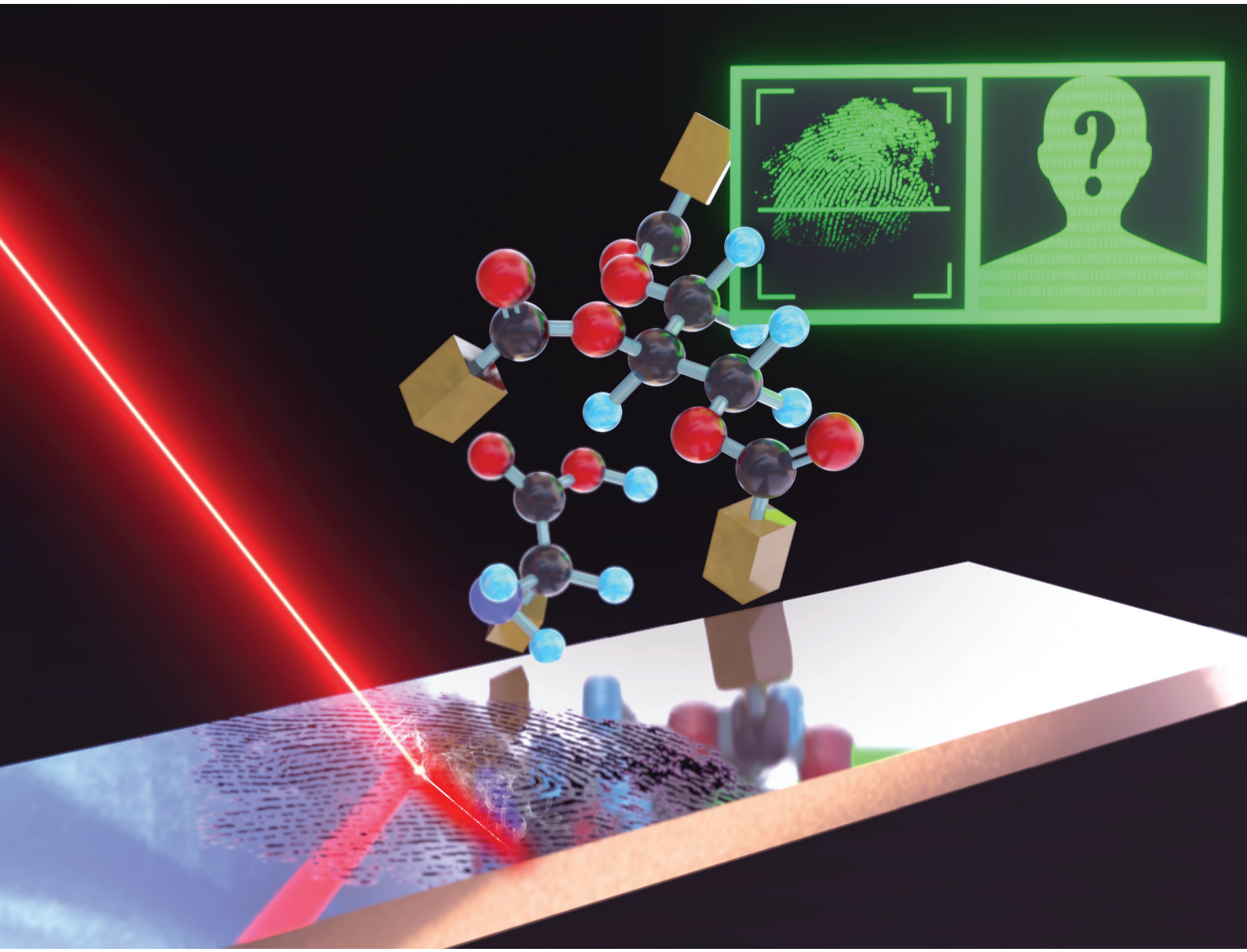

ISSN 0003-2654

ROYAL SOCIETY OF CHEMISTRY

PAPER

Björn van Marwick, Matthias Rädle *et al.*
Rapid chemical detection and segmentation of latent fingerprints by means of a novel middle-infrared scanning method

Analyst

PAPER

View Article Online
View Journal | View Issue

Cite this: *Analyst*, 2024, **149**, 5768

Rapid chemical detection and segmentation of latent fingerprints by means of a novel middle-infrared scanning method

Björn van Marwick, *[a] Tim Kümmel,†[a,b] Felix Wühler, [a] Felix Lauer, [a] Jan Hoffmann[c] and Matthias Rädle*[a]

Received 6th March 2024,
Accepted 4th May 2024

DOI: 10.1039/d4an00367e

rsc.li/analyst

The fast and reliable detection, segmentation and visualization of latent fingerprints are the main tasks in forensics. Currently, conventional fingerprints are searched for, recorded and subsequently analyzed *via* traditional destructive physical and chemical methods. For firmly defined crime objects and undefined crime scenes, the forensic process is very time-consuming and can take several hours for a single fingerprint. In this context, a laser-based measurement technique that records complete latent fingerprints under fifteen seconds in a non-destructive manner was developed that digitizes the fingerprint for postprocessing steps. The optical system is based on confocal measurements in the mid-infrared wavelength range (2 μm–4 μm) to analyze specific chemical substances at crime scenes. The resulting chemical segmentation allows molecule-dependent analysis of latent and visually invisible fingerprints, providing clear conclusions about the perpetrator or the course of the crime. In this study, the application of the developed measurement system (MIR scanner) to capture fingerprints in a molecule-dependent manner within few seconds is demonstrated, compared with reference methods such as FTIR (Fourier transform infrared spectroscopy) imaging, and extended to real crime objects.

Introduction

Ways to find latent fingerprints

The search for and securing fingerprints aid the collection of inculpatory and exculpatory circumstantial evidence to establish a suspect. Fingerprints can identify culprits, prove their presence at crime scenes, establish the manner in which the crime was carried out and determine the intensity of the crime. The dactyloscopic examination of fingerprints includes tasks such as investigating the crime location, seizures, chemical or physical pre-treatment and analysis of the print with a microscope in the forensic laboratory, as well as comparison with a database of digitized fingerprints.[1–4]

Ultimately, the described process determines the quality of the captured image.

Latent fingerprints in the dactyloscopy context

The fact that every individual has a different fingerprint, which does not change, is the basis for legal decision-making and jurisprudence and is fully recognised.[5,6]

The unique three-dimensional pattern of fingerprints is caused by papillary ridges developed on the dermis. This ensures the permanence and stability of fingerprints. Therefore, the pattern can only be modified or destroyed by destroying the dermis.[7,8]

The information contained in fingerprint ridges is processed at three levels.[7,8] The first level classifies the general pattern. Generally, fingerprint patterns can be grouped into whorl, radial and lunar loops, tented arch, plain arch, their combinations, *etc*. For further information, singular points such as the core and deltas as well as the ridge count between the core and deltas are examined more closely.[8–11]

The ridge and valley patterns can exhibit uniquely shaped irregularities called minutia.[12] Minutiae can be ridge endings, bifurcations, convergences, fragments, breaks, enclosures, points or dots, overlaps, crossbars, bridges, opposite bifurcations, docks, trifurcations and returns. These features are developed in the second level and due to scars.[7–9,11]

In the third level, details such as ridge contours or edges, the position and shape of pores, as well as incipient ridges are examined.[8,9]

Most fingerprint recognition systems, such as the automated fingerprint identification system (AFIS), currently use level 1 and level 2 features. Institutions, such as the Federal Bureau of Investigation (FBI), employ various characteristics specified in AFIS image quality specification (IQS) and personal identity verification (PIV) to determine the quality of an

[a]*Center for Mass Spectrometry and Optical Spectroscopy (CeMOS), Mannheim University of Applied Science, Paul Wittsack-Str. 10, 68163 Mannheim, Germany. E-mail: b.vanmarwick@hs-mannheim.de, m.raedle@hs-mannheim.de*
[b]*BASF SE, Carl-Bosch-Straße 38, 67056 Ludwigshafen/Rhein, Germany*
[c]*University of Heidelberg, Im Neuenheimer Feld 440, Germany*
†T. K. was employed by the University of Mannheim during his work on this study and at the time of publication, he is an employee of BASF SE.

image and produce valid matches in their systems. Some requirements set by the FBI relevant to the MIR scanning system to ensure sufficient quality are listed below:

• Pixel density: a suitable image should at least have a resolution of 500 dpi (dots per inch).

• Minimum size: a single fingerprint image must have a length of at least 16.5 mm and a width of 12.8 mm.

• Geometric accuracy describes the distortion of an image generated by the respective recording device. This can be measured by the difference in distance between two points through a calibration target on the image and the real distance between these two points. The geometric accuracy must not exceed 1% for a crossbar and 0.016 for a long bar.

• 256 gray levels (8 bits per pixel) are required.[13–15]

• Depending on the imaging method used for recording and digitization of fingerprints, a physical or chemical pretreatment is performed.[4,16]

To capture fingerprints, physical and chemical methods are used to make direct changes to the sample and contrast it for visualization. Respective examples include the application of graphite powder and chemicals, such as Ninhydrin or even silver nitrate.[17–24] This is in contrast to the non-invasive imaging techniques used to image finger fat, like FTIR, VIS and fluorescence microscopy.[25–31] This also makes it possible to record the fingerprints more than once or by another method. The imaging techniques make use of a physical or chemical property to enable the visualization of the sample.[27–29] For this reason, the chemical composition of the fingerprint is examined in more detail below.

A review of the chemical composition of latent fingerprints

Fingerprints consist of eccrine sweat, apocrine sweat, sebaceous secretions, epidermal substances, and external contaminants.[24,32–34] These substances are present along the papillary lines of the finger and are visible in the form of the pattern created by these lines.

The chemical composition of the secretion, as well as the number of sweat glands, can vary between people and the body parts studied. This also depends on the physical condition of the subject.[35–39] As a result, the chemical composition of a fingerprint may also change. Therefore, it is necessary to consider not only the whole fingerprint but also the composition of its individual components.

The main component of eccrine sweat is water, along with various electrolytes, such as sodium, chloride, potassium, calcium, and magnesium, dissolved in it. It also contains lactate, ammonia, amino acids, glucose, urea and bicarbonate, as well as various peptides and proteins.[36,38–44]

Apocrine sweat is an oily secretion containing proteins, lipids and steroids. As the sweat is secreted at the hair root the same way as the sebum, their ingredients are tricky to differentiate as they can easily get mixed up. The components of apocrine sweat include amino acids conjugated with carrier proteins of pheromones, sugars, electrolytes, urea and ammonia.[39,42,44,45] By selecting appropriate wavelengths, scanners can be tuned to record the absorption of all listed substances in the eccrine and apocrine sweat. Exceptions are the electrolytes, which do not show NH and CH absorption bands. The other substances show an absorption band in at least one of the ranges.[46–58]

Sebum is composed of glycerides, free fatty acids, wax, esters, squalene, cholesterol esters, and cholesterol. It constitutes a major part of the secretions present on the skin surface.[23,59–65] Free fatty acids are fatty acids with an acid residue containing long-chain CH bands of up to 18 members.[61,63,64]

Similar to sebum, the epidermal substance of the skin is composed of molecules with long-chain CH bands as well. It consists of lipids, such as triglycerols, free fatty acids, sterols and phospholipids.[66–68]

Current analytical methods of fingerprint detection and development

Especially, fingerprints that cannot be transferred to the laboratory for development are often treated with a contrasting powder. This powder is available in different colours for subsurface contrasting as it can be dyed with fluorescent particles, and also is magnetic for easy application. After physical application, the fingerprint is fixed to a carrier card with duct tape and transferred to the laboratory.[17,18,20,69,70]

Another traditional technique is chemical fingerprint development using ninhydrin, DFO, crystal violet, silver nitrate, cyanoacrylate, amido black, ardrox dye and other chemicals. The goal of these methods is to increase the contrast of the fingerprint with respect to the background. The contrast agents themselves form a chemical bond with one or more components in the fingerprint, causing a change in the physical properties of the fingerprint. These can manifest as a change in the colour impression or fluorescence. However, most of these chemicals are harmful to human health.[17,20,21,69–80]

Established imaging methods for chemical and forensic tracing

Since handling harmful substances is difficult, other methods like imaging are also used to digitize fingerprints and compare them with databases. Most of these imaging methods are non-invasive, which means that the analysis is non-destructive and does not cause any changes to the sample. However, in visual microscopy and fluorescence microscopy, contrasting agents or markers are often used in the sample preparation process. This can change both chemical and physical properties to induce a desired effect, such as fluorescence, or enhance the contrast in conventional microscopy. The disadvantage of this is that the modified sample may no longer be usable for further analysis.[25,29–31,69,81–87]

The advantage of examination by fluorescence microscopy is that fingerprints can be examined for certain molecule groups by using a suitable contrast medium. However, only those corresponding to the contrast agent can be examined. The natural fluorescence signal of organic substances in the fingerprint is too low for recording and negatively influences the image recorded using contrasting agents.[30,31,87,88]

Fourier transform infrared spectroscopy (FTIR) is a non-invasive method that evaluates the vibration bands of specific molecular groups. The peak position in the recorded spectra provides information about the molecular group and the intensity denotes layer thickness and concentration. The sample is scanned pixel by pixel, and a complete infrared (IR) spectrum is recorded. Afterwards, the wavelengths of the corresponding chemical groups can be selected and compared with each other. This contrasts the fingerprints that differ chemically from the background. The disadvantages of this method are high image acquisition time (~30 min per cm^2) and the need for IR marking to increase the acquired optical signal of the fingerprint components to achieve sufficiently high contrast. Thus, this method is often associated with long acquisition times and increases with the sample size or higher resolution.[29,81–86]

Similar to FTIR, Raman microscopy measures molecule-specific vibrational bands. However, this is done using high-power excitation and detection of the resulting inelastic scattering. For this purpose, the signals must be distinct from the excitation wavelength and not in the immediate vicinity of the excitation, as the molecule-dependent Raman bands are easier to identify spectrally than the infrared bands. This allows the subtraction of background polymer bands without the loss of analyte information even on porous or granular surfaces. In contrast, FTIR tends to favour reflective surfaces in order to display distinct contrast. The disadvantages of the described measurement technique are acquisition speed, mostly poor spatial resolution and low sensitivity.[81,83,89–92]

More advanced strategies, such as matrix-assisted laser desorption ionization, can be used to characterize specific substances. This presents an advantage over traditional measurement techniques that can only identify chemical groups. The disadvantages of this method are high initial cost, long image acquisition time, very limited measurement area, the destruction of measured samples, and highly complex interpretation of the recorded data. Often other imaging methods are used upstream to record the region of interest. Therefore, this method is often used when information beyond the fingerprint itself is of interest, such as for the analysis of residual traces of drugs.[93,94]

Chemical challenges posed by different surfaces

Due to the chemical challenges in contrasting fingerprints from different surfaces and the variability of sample yield with relevant fingerprints, all measurement methods can outperform the others in certain applications. While the difference between reflective, transmissive and colored subsurfaces can directly benefit or exclude certain options, the measurement conditions can be complex. Another issue is the nature of the substrate. As the roughness and porosity of the substrate increase, optical measurement becomes more complicated and inefficient due to scattering effects. Three-dimensional patterns can also cause local resolution differences, which also negatively affect the final result. Likewise, the accessibility of the fingerprint to contrast agents is not always guaranteed and is dependent on the substrate. Fingerprints can be on hidden surfaces that are not accessible without considerable effort. Practical examples include taped envelopes, plastic bags and packages associated with the crime. Pulling the tape off the surface can directly cause the destruction of the fingerprint. There is great interest in the forensic evaluation of the adhesive layer of the tape because a fingerprint is left on the adhesive layer when the tape is pulled off and re-applied. Since the adhesive tape then adheres to another layer or to itself on this side, it is difficult to gain non-destructive access to the fingerprints. Refrigerants can be used to remove the adhesive tape as it allows better preservation of the traces compared to careful peeling without tools or solvents. Thermal heating deforms the sample and thus cannot be used for peeling. With increasing access to liquid nitrogen and oxygen at forensic facilities, quick freezing and thawing of small areas are often used to detach adhesive layers. Although the technique is simple to perform, it requires experience and practice to handle the refrigerants because they are capable of instantly freezing even living tissues and skin. Appropriate protective equipment, especially for the eyes and hands, must also be worn during this procedure. By this method, it is possible to remove adhesive strips even from dead victims without tissue damage. Common methods include immersing the sample in liquid nitrogen or applying it using a cryo-applicator. In the rarest of cases, however, it is still possible to remove the tape completely without alterations. In case of alterations a fingerprint can often no longer be developed appropriately. Depending on the material, it may also be advantageous to use a solvent. This depends on the situation, and therefore, a material test is necessary before method selection.[95–97]

Given the disadvantages of this method, including a limited field of application, long acquisition times and large data sets, a new type of measuring instrument based on the principles of FTIR has been developed in recent years. In this case, the scanning system is used to contrast latent fingerprints under different conditions.

Material and methods

Novel measurement method for rapid latent fingerprint detection

The developed laser-based measuring system is specially designed for the detection of lipid- and protein-containing substances. The measuring technique involves measurement at several wavelengths to detect the absorbance of the substances and the local scattering properties of the sample or sample substrate. The scattering properties are important to measure the general optical influence on the sample and are used as references for absorption measurements.[98–102] Therefore, a wavenumber with low absorption is used. The measured absorption properties of the sample directly correlate with chemical properties. This is because the energy provided to the molecule by a light beam can be converted in different ways, such as thermal conversion, and vibration or

rotation energy. As the vibrational energy of a molecule is described by its quantum number, it can only take molecule-specific values. The converted energy corresponds to radiation energy and is, therefore, dependent on the wavenumber. To achieve radiation energy matching the vibrational energy, the radiation has to be in the range of 12 800–200 cm^{-1}. If the energy provided by radiation is not sufficient, the molecule converts it into rotational energy, which is also quantised again and thus is dependent on the wavenumber. Vibrational or rotational movement can also be associated with the movement of electric charges, which are not necessarily distributed symmetrically in the molecule or can become asymmetrical due to vibrations. Accordingly, infrared radiation with a suitable wavenumber has an effect only on atomic groups in which dipole moment changes happen or are brought about by antisymmetric vibrations.[83,99,103,104]

The wavenumbers of the scanning system were, therefore, selected for common molecular groups found in organic samples, such as the valence vibrations of CH_2 (2926 cm^{-1})[105] and NH (3200 to 3570 cm^{-1})[106–108] groups.

The laser wavenumbers were, therefore, selected as follows:

- Laser 1: detection of the scattering properties of lipid structures with wavenumber 2790 cm^{-1}.
- Laser 2: detection of the absorption properties of lipid structures with wavenumber 2926 cm^{-1}.
- Laser 3: detection of the absorption characteristics of protein structures with wavenumber 3350 cm^{-1}.
- Laser 4: detection of the scattering properties of protein structures with wavenumber 3700 cm^{-1}.

By detecting both scattering and target signals, it is feasible to compute and mitigate the influence of suboptimal background conditions because scattering signals reflect the irregularities and surface roughness of the observed substrate. These irregularities also manifest as interference signals in the image acquired at the absorption wavenumber. Using the Lambert–Beer calculation, it is possible to effectively eliminate these interference signals from the absorption image, thereby facilitating enhanced contrast and clarity of the sample. The associated chemical segmentation of the fingerprints is then based on four selected wavelengths in the IR wavelength range and not on the whole IR spectrum like FTIR imaging.

The collimated laser beams illuminate the sample sequentially and pass through an optical lens system, which expands and finally focuses the corresponding laser beam onto the sample. In the process, the light beam is deflected linearly over the sample by moving the agile mirrors in the scan system. The sample then moves orthogonally to the generated laser line, achieving a rectangular measurement field. The movement is facilitated by a microscope stage. The spectrum is recorded confocally using a single-photon detector attached to a computer unit and the image is obtained based on calculations. As shown in Fig. 1, a linearly moving mirror aligns the lasers one at a time with the optical lens system.

The laser light, beam guidance and the confocal arrangement of the IR detector in combination with the sample movement enable extremely short measurement times of up to three seconds per cm^2 for each laser. The spatial resolution is 20 μm. However, these measurement times are only possible due to the optical properties of the lenses used (CaF_2 and BaF_2), mirrors (gold-coated) and the highly sensitive IR detector ($D^* = \sim 4 \times 10^{-10}$ cm $Hz^{1/2}$ W^{-1}). This is because, at a high speed, the exposure time of the IR detector is very low (5 ns). Therefore, only minor losses through optical components can be tolerated as confocally measured absorbance can only be acquired in the sensitivity range of the detector unit.[109–111]

As mentioned in the introduction section, all chemical substances present in the sebum and epidermal substance exhibit a CH absorption peak in the range of the wavelength used.[81,82,112–120]

In confocal measurements, it is important to record the scattering signal when the sample surface is not perfectly smooth because the measured signals of rough surfaces are more influenced by light scattering than the intended direct reflection. Therefore, the direct reflection of uneven surfaces cannot be measured, which results in a drop in the signal. In order to record the fingerprint found in difficult background conditions, it is, therefore, necessary to offset the signals of the scattering properties.

As most components of fingerprints consist of functional CH_2- or NH-groups, the IR spectra of all components will exhibit absorption peaks at least for one of the selected lasers. Since externally ingested substances vary from case to case, no precise analysis can be made on this. Nevertheless, the above functionality test verifies that the scanner covers a wide range of organic substances, including some externally ingested substances. The organic substances also visualize for the spectra of the fingerprint itself. Therefore the the scanning system described in the following is able to detect both fingerprints and their components.

Sample preparation and measurement conditions

For basic comparative measurements between the MIR scanning system and FTIR imaging, the fingerprints were applied

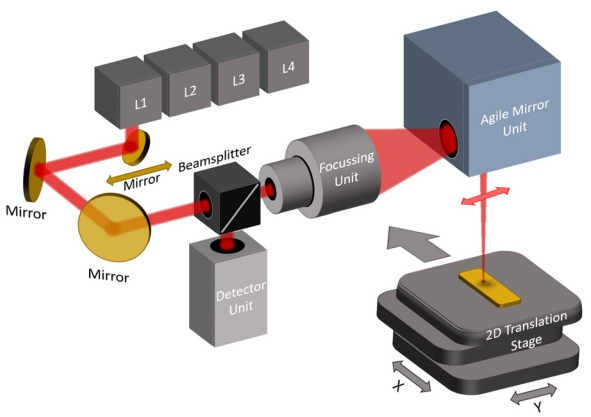

Fig. 1 Schematic of the MIR scanning system with inbuilt lasers of wavenumbers 3700 cm^{-1} (L1), 3350 cm^{-1} (L2), 2926 cm^{-1} (L3) and 2790 cm^{-1} (L4).

to gold-coated (MN10-AU8632, Science Services GmbH, Germany) or silver-coated (MirrIR Low-e Corner frosted, Kevley Technologies, Ohio) slides. This is due to the nearly ideal reflectivity of both substrate substances, which ensures comparability between the measurement methods. This research was approved by the Medical Ethics Committee II, Faculty of Medicine, Ruprecht Karl University of Heidelberg (approval number 2024-620). All procedures were performed by following the institutional guidelines, along with any applicable national and international regulations. Patient information and consent were obtained in compliance with the guidelines set by the ethics committee (guaranteeing adherence to the Declaration of Helsinki).

To investigate the effect of problematic substrates, sample carriers made of other materials commonly found in weapons or similar to their composition were also prepared. An aluminum sheet with a thickness of 3 mm was cut to 25 × 75 mm samples. A plastic card from the Mannheim University of Applied Sciences was also used. With this, comparable results to a German identity card were achieved. In order to protect the holders, only the results of the plastic card described and not those of the ID card are published. Furthermore, a wooden tongue depressor (wooden tongue depressor, Zarys, Poland) was sprayed with clear varnish (3468683, OBI, Germany) and cut to a length of 75 mm after the varnish had dried. Another untreated wooden tongue depressor (wooden tongue depressor, Zarys, Poland) was also cut to 75 mm. A paper sheet, a dollar note, as well as the plastic card and the wooden tongue depressors, were each taped onto a silver-coated glass slide (Carl Roth GmbH+ Co.KG, Germany). After this step, all sample carriers were cleaned with 99% ethanol and air-dried. A fingerprint was then applied to all sample carriers and examined the next day using the FTIR and MIR scanners.

Scotch tape (TESA SE, Germany), insulating tape (TESA SE, Germany), duct tape (3M 1900, Germany) and parcel tape (TransPak AG, Germany) were cut into 15 × 25 mm pieces to create the required sample carriers. Disposable gloves were worn during this process to avoid leaving any traces on the samples during preparation. A fingerprint was then applied to the sample carriers and they were respectively applied to a silver-coated object carrier. Then, the samples were examined first using the FTIR system and then the MIR scanner.

For examination with the MIR scanner, the recorded fingerprints were placed in the sample holder of the measuring device. The sample was then moved into the measuring range of the instrument in an automated manner. The sample was sequentially scanned with all four laser wavelengths. Then, the resulting measurement points were calculated to form an image that was used for further image processing and analysis. Due to possible inaccuracies while transferring the lasers into the optical path of the system, the scanner results may have an offset. This was recorded using a calibration target (Edmund Optics, Germany) and compensated by moving the microscope stage in the system. This target moved with precisely 5 μm more positioning accuracy than the resolution achieved later. The successful implementation of this calibration target was then validated.

For fingerprint examination by FTIR imaging, the measuring instrument (Spotlight 400, PerkinElmer) was precooled in advance using liquid nitrogen for ~35 min. Subsequently, the sample was moved by hand to the desired measurement area and then focused. An overview image (measurement time per cm^2 ~20 min) was then used to more concretely delimit the area of spectral measurement (generation of a region of interest; ROI). After subsurface measurement, the areal spectral survey of the samples was obtained. In our experiments, the spatial resolution was 25 μm, the spectral resolution was 16 cm^{-1}, and the travel speed of stage movement between two measurement points was 2.2 m s^{-1}. In combination with an accumulation of a factor of 10, this allowed samples to be measured at a time of ~30 min per cm^2. The spectral measuring range was limited to 750 cm^{-1} to 4000 cm^{-1} per measuring point. The intensity of the sample was measured by direct reflection. Further, a reference measurement was carried out on a gold-coated slide before the actual scan. This was used by the FTIR device to calculate an absorption spectrum for every measured pixel.

Algorithms and data (pre)processing

The two-dimensional scan field was drawn up by a deflection of the agile mirror unit in the system and a movement perpendicular to it through the microscope stage. Image distortion was reduced by adjusting the speed of the described components. Synchronisation between the deflection units and signal processing in the detector was achieved by using a mathematical correlation to trigger data acquisition depending on the deflection of the laser beam and displacement of the microscope stage. During the scanning process, pixels were generated with a sampling rate of up to ~2.7 MS s^{-1} (including oversampling). The number of pixels determines the number of measuring points during the scanning process. The number of measuring points during the scan does not correspond to the final number of image points, as oversampling leads to better imaging results. Thus, ten measuring points were averaged to obtain one image point.[110,111]

To generate absorption-based images, it is necessary to offset the scan images obtained using the reference laser with the scan images captured using the target laser. For this purpose, each pixel of the two images was correlated with each other according to the Beer–Lambert law.[99,121,122]

$$A = -\log\left(\frac{I}{I_0}\right)$$

Therefore, two images, one target and one reference image were used to obtain each absorption-based image.

Due to deteriorating measurement conditions in this study, measurements were carried out in the noise range of the detector. In addition, the intensity decreased horizontally from the center with greater deflection of the laser. These effects mean that clear contrasting is only possible with difficulty during target measurement under difficult conditions. This can be

improved by mathematical correction of the image data. For this purpose, fifth-degree polynomial regression was carried out for each horizontal data set and subtracted to obtain the difference. This normalization step reduced the gradient formed in the image due to signal drop and the intensity gradient between individual horizontal data sets caused by detector noise. This correction only improved the data recorded using the MIR System but not the FTIR system.

Results

A proof of concept: challenging common imaging methods

For the spectral measurement of latent fingerprints, four fingerprints were applied to gold-coated slides under different conditions. One of the fingerprints was applied without physical exertion and one after an hour of jogging. Another fingerprint was applied after wetting the finger with adeps lanae anhydricus (Caelo, Art. Nr. 3010), which is a contrast agent for the lipid band in the mid-infrared range. The last fingerprint was contrasted with previously drawn blood. The fingerprints were measured one day after they were applied on the slides to allow evaporation of any residual moisture or water and exclude the possibility of interference with the spectrum. The analysis of vibrational bands relevant to this study would otherwise not be possible as the vibration band of water overlaps with the bands of interest.[123–125] This issue of fingerprints being overlaid by moisture would not only be visible in the spectra of the FTIR scans but the difference in intensity levels within the images acquired with the MIR scanner would also be displayed. As this was not the case, disruptive effects due to moisture could be ruled out in our samples.

To evaluate the spectral data, especially, the NH band at 3350 cm^{-1} and the CH band at 2926 cm^{-1} were examined.

The peak of the NH band was more pronounced in the fingerprints contrasted with blood and after physical exertion than in the normal fingerprint, as shown in Fig. 2. According to the literature, sweat increases the concentration of amino acids in the fingerprint, which explains this difference in intensity.[36,38–44] The proteins and amino acids in the blood also ensured an extremely high intensity of the NH band.[126,127] This peak was not recognizable in the spectra of the adeps-lanae-enhanced fingerprint.

The peak of the CH band was visible in the spectra of every fingerprint. The fat-enhanced fingerprint showed the highest intensity as it is a contrast agent for this absorption band.[128,129] The other spectra showed very close CH- peaks, with the fingerprint imprinted after exertion showing the lowest intensity. This could be the result of some fingerprint components being washed away by sweat.

The characteristic peaks of the NH and CH bands respectively at 2926 cm^{-1} and 3350 cm^{-1} also varied in intensity within the fingerprint, as shown in Fig. 3 and 4. The normal fingerprint showed areas where both CH and NH bands were dominant. This indicates that chemical differences within the fingerprint are recognizable by this approach.

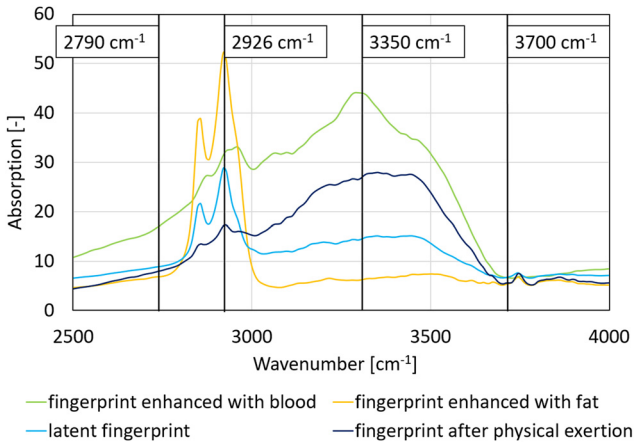

Fig. 2 FTIR spectra of a latent fingerprint, a fingerprint enhanced with blood, a fingerprint enhanced with fat and a fingerprint after physical exertion.

The differences in intensity of the NH band indicate that incorporating this wavenumber in the scanning system enhances the quality of acquired data and data load. Adding the NH band for more chemical information enabled better contrast against the background. Before validating this added value, a comparison was first made between the developed scanning system and FTIR. For this purpose, in the FTIR data, the intensities observed at wavenumbers used in the mid-infrared scanner were calculated according to the Beer–Lambert equation to visualize the layer thickness and concentration of the CH bands or NH bands within the latent fingerprints according to the absorbance values. The absorption-based images showed the latent fingerprints based on both vibration bands in contrast to the background. On closer inspection, however, it was noted that the intensities varied within the traced papillary lines due to differences in their concentration and layer thickness within the fingerprint. The MIR system was also used to record all four samples using the four lasers, and differential images of the two bands were created according to the Beer–Lambert equation.

Rapid chemical segmentation of latent fingerprints on different surfaces

In order to compare the differences in contrast between the two measurement methods and to understand their limits, fingerprints were applied to different surfaces. The surfaces used were aluminum, a plastic card, coated and uncoated wood, a currency note and paper. The selection of substrates was based on the frequently used crime weapons.[130,131] The materials used as surfaces are similar to those found in weapons. In addition, the reflectivity of the selected materials was different. In the first step, the highly reflective substrates, including aluminum and plastic card, were examined. In this study, aluminum delivered comparable results to stainless steel, for example. It is, therefore representative of metals with a higher degree of reflectivity in the mid-infrared range, including gold, silver, aluminum, copper, platinum, rhodium,

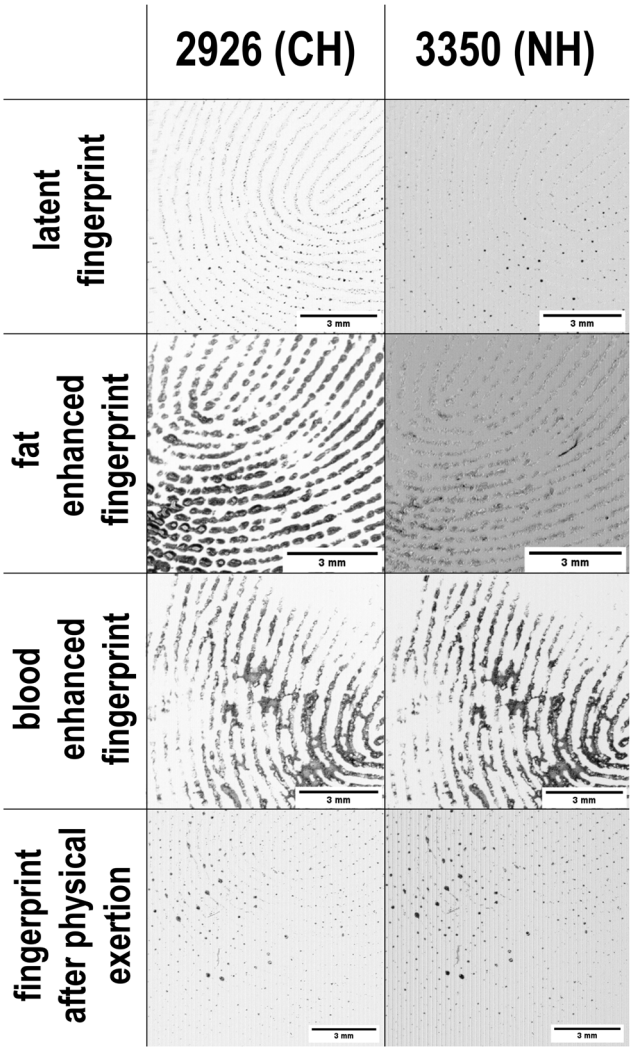

Fig. 3 Images acquired based on the CH and NH absorbance bands of a normal latent fingerprint, a fingerprint enhanced with blood, a fingerprint enhanced with fat and a fingerprint after physical exertion scanned using the FTIR system.

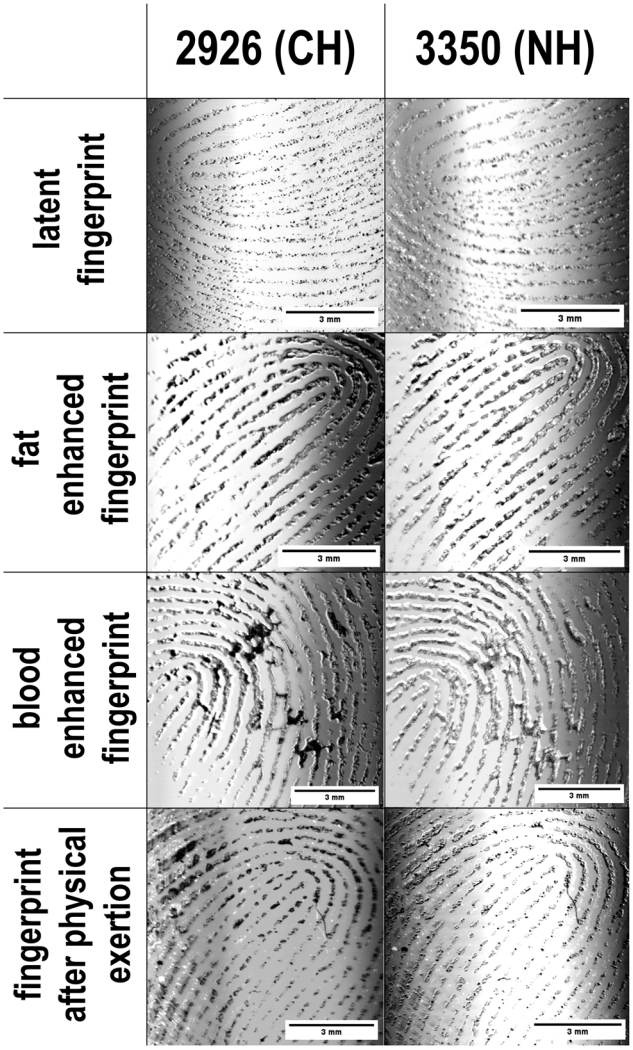

Fig. 4 Images acquired based on the CH and NH absorbance bands of a normal latent fingerprint, a fingerprint enhanced with blood, a fingerprint enhanced with fat and a fingerprint after physical exertion scanned using the MIR system.

tungsten, chromium, vanadium, iron and magnesium.[132,133] The plastic card showed scanning results similar to a German identity card. On the grounds of discretion, these details are not published in this study.

The measurement of fingerprints on various substances using the FTIR imager and the recently developed MIR scanner is discussed below. In the FTIR scans, the fingerprint could only be contrasted weakly from the background for most of these surfaces. Especially, the fingerprint on the plastic card displayed a clear contrast with respect to the CH band. As seen in Fig. 5, the others were barely visible.

With the MIR scan, all the bands presented reliable contrast for the fingerprints on the aluminum and the plastic card surface, as shown in Fig. 6.

Next, substrates with non-reflective surfaces, including standard glass slides (Carl Roth GmbH+ Co.KG, Germany) and wood (wooden tongue depressor, Zarys, Poland) coated with clear lacquer (3468683, OBI, Germany), were examined. These fingerprints showed weak contrast when scanned by the FTIR device, as shown in Fig. 5. This is comparable to the aluminum substrate. The strongest contrast was from the CH bands of coated wood. The contrast obtained with the MIR system was much higher. The fingerprints were visible on the glass slide, as well as coated wood.

In the last step, fingerprints were applied to substrates without a reflective surface but were chemically composed of many CH and NH groups to mimic more difficult scanning conditions and also show the limitations of the two scanning systems. The chosen substrates were wood (wooden tongue depressor, Zarys, Poland), paper and a US-dollar note. Fig. 5 shows that no fingerprints measured using the FTIR system showed contrast. Only the impressions on the dollar note were visible. In comparison, Fig. 6 shows that the MIR scans enabled the visualization of the fingerprint on paper. On wood

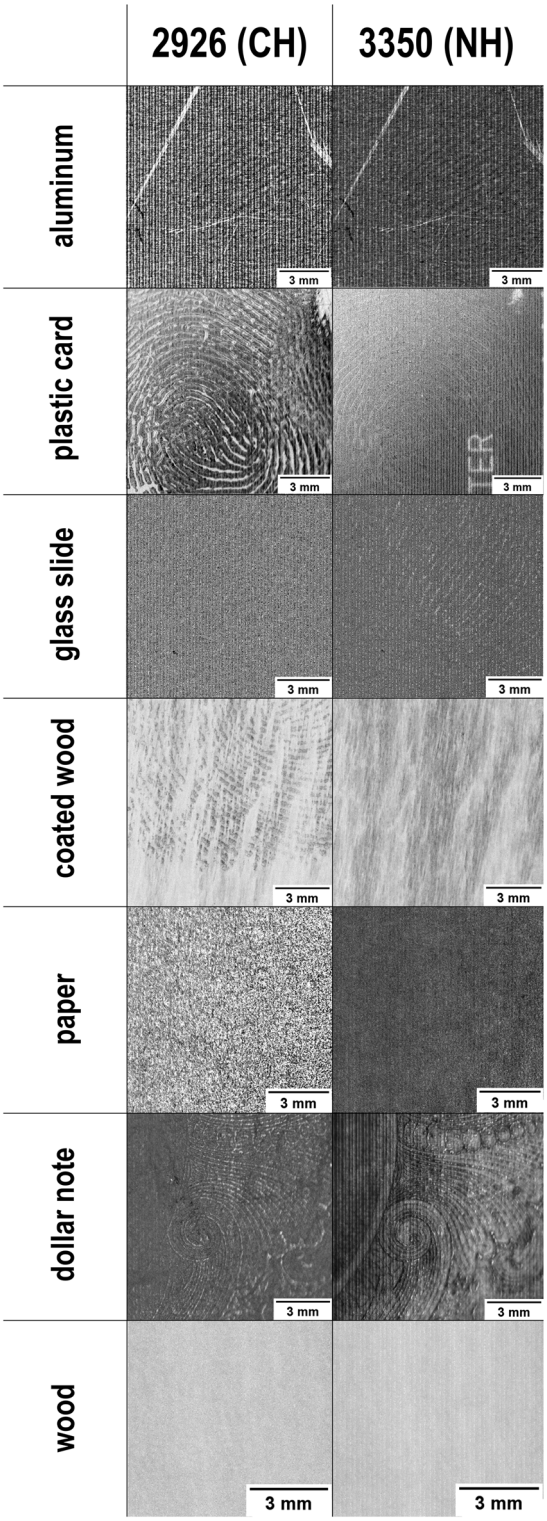

Fig. 5 Images acquired based on the CH and NH absorbance bands of latent fingerprints scanned on aluminum, a plastic card, a glass slide, wood (coated and uncoated), a dollar note and paper using the FTIR system.

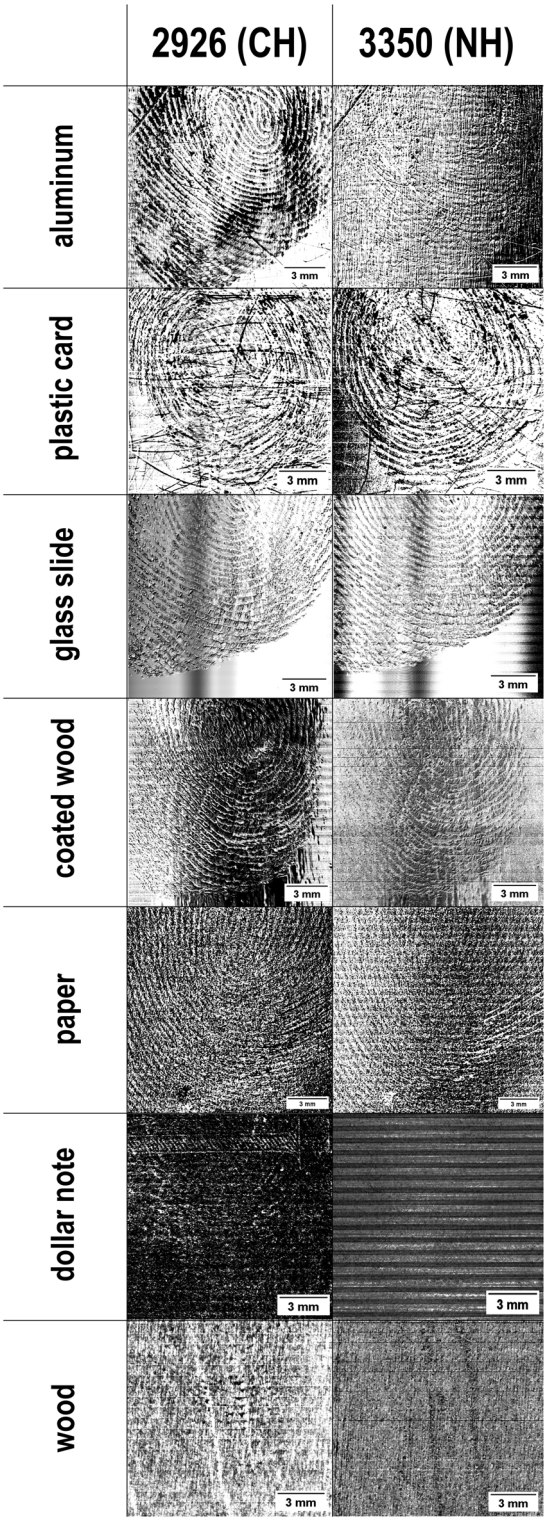

Fig. 6 Images acquired based on the CH and NH absorbance bands of latent fingerprints scanned on aluminum, a plastic card, a glass slide, wood (coated and uncoated), a dollar note and paper using the MIR system.

and the dollar note, only a part of the fingerprint was visible. Although the contrast was not sufficient for automated evaluation by software, the images still clearly showed the differences between the contrast ratios of the two systems, suggesting that the MIR scanner outperforms the state-of-the-art FTIR spectroscopy.

Imaging hidden latent fingerprints on chemically similar substances

In general, fingerprints can only be obtained from surfaces. Therefore, traditional chemical or physical dactyloscopy methods for retrieving fingerprints are not suitable for covered fingerprints. In our study, we assumed a case where fingerprints are located on tapes that are tightly adhered to a surface.

As mentioned in the introduction, the process of obtaining fingerprints located on tapes is intricate. We investigated the capability of the measurement method developed here in detecting fingerprints on adhesive layers adhering tightly to a surface.

In this pre-study, the adhesive layers used were common transparent scotch tape (TESA SE, Germany), insulating tape (TESA SE, Germany), duct tape (3M 1900, Germany) and parcel tape (TransPak AG, Germany). A fingerprint was applied to the side of the adhesive layer, and the tape including the fingerprint was fixed to a MirrIR slide. Thus, the fingerprint was located between the substrate and the covering plastic layer. Importantly, the tape was not smoothed out after its application to avoid the destruction of the fingerprint. The resulting trapped air bubbles would make it difficult to measure the fingerprint homogeneously. However, a forensic scientist must also deal with these factors at the crime scene.

The measurement results in Fig. 7 show the results recorded by the FTIR system. No fingerprint could be recognized under the duct tape and parcel tape. The fingerprint under the common transparent scotch tape was weakly contrasted, suggesting that clear identification of the person can probably not be guaranteed afterwards. Only the fingerprint under the insulating tape was well contrasted.

Fig. 8 shows that the mid-infrared scanner was able to clearly contrast the fingerprint under the scotch tape in addition to the insulating tape. Another striking feature was the images formed from the NH absorbance bands. The added value of the additional laser pair found in the proof of concept was observed again, in which the fingerprint under the parcel and scotch tape could be recognized more clearly than the images based on the CH absorption bands.

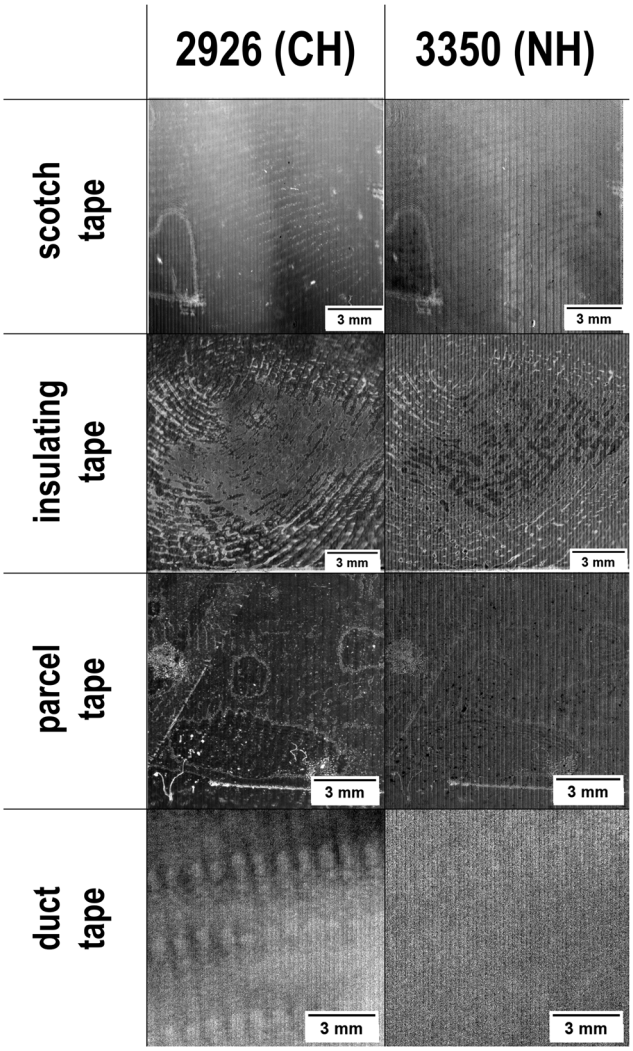

Fig. 7 Images acquired based on the CH and NH absorbance bands of latent fingerprints between a MirrIR slide and scotch tape, insulating tape, duct tape and parcel tape scanned using the FTIR system.

3D latent fingerprint visualization depends on chemical information from the middle-infrared range

In forensics, in addition to the distance between individual papillary lines and their width, the layer thickness can also be used to convict the perpetrator.[134,135] The extraction of height information contained in a fingerprint can therefore be an advantage in identification.

Due to the existing correlation between light absorption and layer thickness, it is possible to extract height information from the recorded absorbance values. To realize this, a model was created for clear height assignment to the recorded absorption values. For this reason, adeps lanae used in the earlier experiments was coated onto a microscope slide. In order to assign height values to the coated adeps lanae, a wedge was produced using Computer Aided Design (Autodesk Inventor) to be used as an application aid during coating. This was 3D-printed with a resin printer (Black Standard Resin, Form3, Formlabs Inc., USA) at a resolution of 25 μm. The wedge had a height gradient of 200 μm down to 1500 μm over a distance of 50 mm. A homogeneous coating of grease is only achievable only under heat as high-viscosity coatings can cause unevenness of the surface. Adeps lanae was heated to 70 degrees and then coated at room temperature so that it had a low viscosity during coating but also hardened quick enough to avoid running. The resulting adeps lanae wedge was scanned several times with the CH band lasers, and multiple samples were produced to check for data reproducibility. The data was averaged over their positions on the fat wedge, and the standard deviation was determined. The intensity values plotted over the height show a logarithmic correlation in Fig. 9. In order to calculate the intensities, their offset was determined by measuring a pure gold slide.

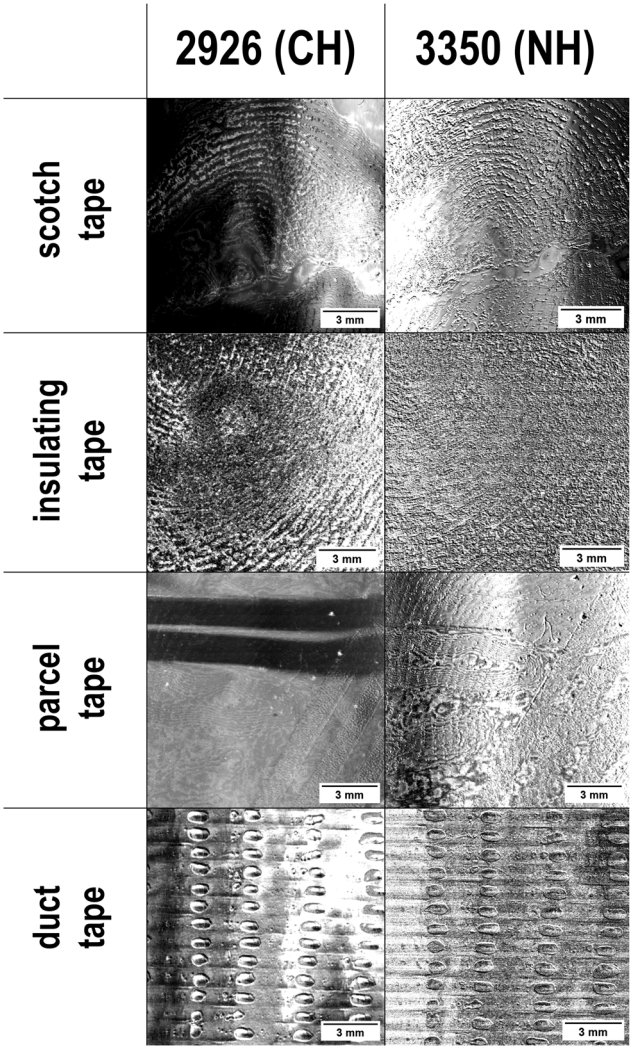

Fig. 8 Images acquired based on the CH and NH absorbance bands of latent fingerprints found between a MirrIR slide and scotch tape, insulating tape, duct tape and parcel tape scanned using the MIR system.

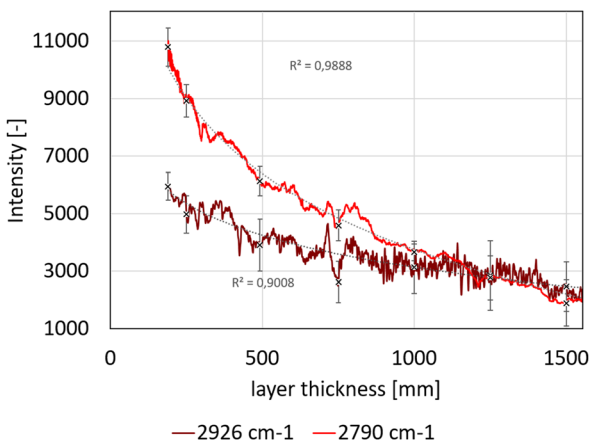

Fig. 9 Logarithmic intensity correlation with different layer thicknesses of adeps lanae scanned using the MIR system.

After calculating the absorption from the measured intensities, a linear slope was obtained as expected. Because of small surface variations, as well as gloss effects influencing the data, a median filter was applied over ten values for each calculated adsorption. Ten values represented 0.2 mm of the scanned area. As the influence of gloss and surface defects is at a larger scale, this calculation does not eliminate all outlier values. As shown in Fig. 10, the graph showed a regression of 0.9024. The model was then applied to a fingerprint scanned at the same scan settings.

It is important to use the same scan settings as when creating the model. With the adjustment of the gain the output signal of the detector can be modified for better contrast in the imges. This means that the height assignment no longer fits. Therefore the detector settings influence the absorbance and signal correlation. The scanned and calculated fingerprint on a silver-coated slide was characterized by a height profile between 0 and 400 µm, as shown in Fig. 12.

However, it was found that individual outliers also went beyond this limit, as visualised in Fig. 11. This may be due to

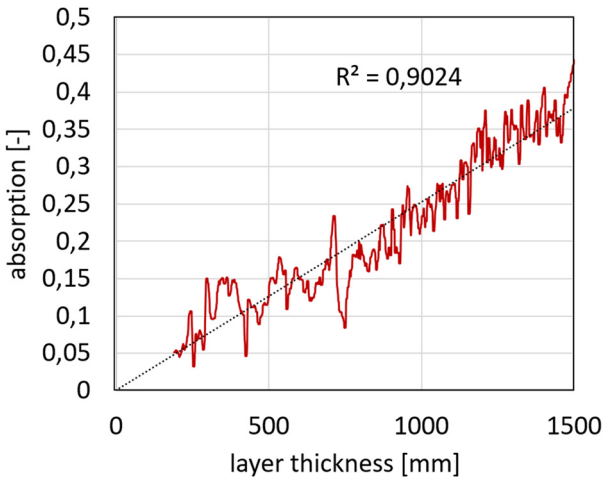

Fig. 10 Linear absorbance correlation to different layer thicknesses of adeps lanae scanned with the MIR system.

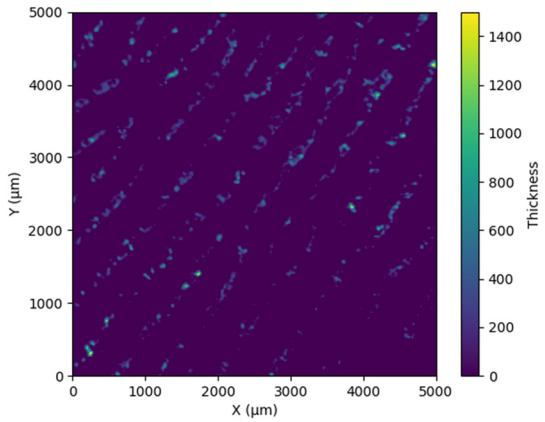

Fig. 11 3D image of a latent fingerprint obtained by converting the absorbance values from the MIR system to layer thicknesses with the help of the calculated model.

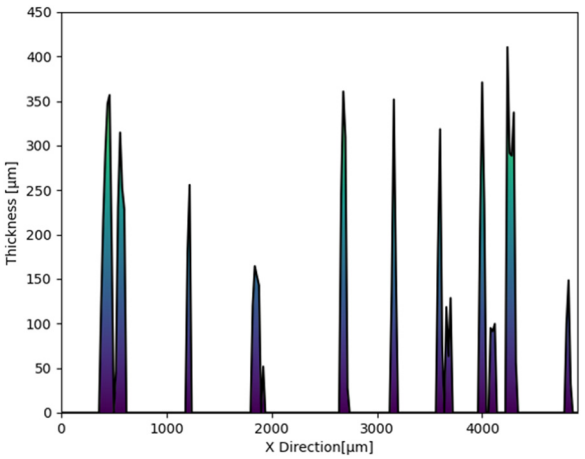

Fig. 12 Layer thickness of a latent fingerprint calculated using the absorbance values obtained with the MIR system and plotted over a virtual line in the middle of the latent fingerprint.

dust particles or impurities that cause interference effects during measurements.

According to the literature, a fingerprint should only be a few µm thick.[136,137] The observed differences can be attributed to the transfer of adeps lanae to the finger fat. In this study, it has already been shown that their spectra not only differ in intensity but also that the concentration varies depending on variations in layer thickness within the fingerprint.

Conclusions

Faster scanning to obtain high-contrast images that can even contrast latent fingerprints found in difficult measurement conditions are the main advantages of the developed MIR System. Moreover, sample preparation does not require contrast agents, which are very harmful to health and need to be handled with appropriate precautions. A chemical distinction between the background and latent fingerprint eliminates the influence of background structures do on the final result unless their chemical structures are similar and thus simplifies subsequent image evaluation. The main problems with common mid-infrared technology are low contrast and long acquisition time to visualize samples. With a scanning time of 3 seconds per laser, the new scanning system allows sample visualization up to 60 times faster than FTIR. Notably, the detector of the mid-infrared system uses electrical cooling, whereas, the FTIR device has to be cooled with liquid nitrogen. This means that the mid-infrared scanner can measure immediately when switched on, whereas, the FTIR system must first be cooled down to a suitable measuring temperature using liquid nitrogen. Further, wrong cooling can lead to bad scan results, which is avoided in the MIR scanner as electrical cooling is very accurate. The MIR scanning system acquires only a small part of the whole spectrum. On the one hand, this provides less chemical information but also means data post-processing requires less effort. On the other hand, the lower chemical information provided by the mid-infrared scanner can also be a disadvantage. In comparison, FTIR provides a whole spectrum that can be used to analyze unknown samples even if they do not have peaks in the region of the CH or NH bands. Achieving contrast against chemically similar substrates becomes more difficult if fewer absorption bands are included in the calculation. With a whole spectrum, all peaks can be taken into account for calculations. As this is not possible with the MIR scanner, additional absorption bands, such as the NH bands, can provide additional or even completely new information about the sample. This makes a difference, especially in the visualization of targets with higher protein concentrations. The advantage of integrating additional wavelengths is limited by the availability of strong absorption bands. In the investigated range, this availability is exhausted by the two bands used for detecting latent fingerprints. In the mid-infrared range of the fingerprint spectrum, there are other bands that can also be used, but they do not have comparably high intensity for lipids as the ones used. This limits the value of adding further bands and adds structural difficulty because the spectral range of the detector does not cover them. In this study, the value of the additional NH vibration bands was visible in the blood- and sweat-enhanced fingerprints, and especially in the fingerprints hidden under scotch and parcel tapes. Further, it enables the visualization of fingerprints on surfaces with difficult scanning conditions except for wood and the dollar note. The contrast provided by the new scanning system is also superior to FTIR, which is currently regarded state-of-the-art. As for powerful lasers and a detector specifically tuned to the required wavelength range, the detectivity in the range used is higher (7×10^{11} cm $Hz^{1/2}$ W^{-1}) than the broadband detection range of FTIR. The results demonstrate that the samples on paper, aluminium, glass and coated wood, which cannot be seen at all with FTIR or can only be visualized very poorly, show significantly better results with MIR. The MIR scanning system only shows limitations with the samples on wood and the dollar note. The extent to which the other samples can be evaluated using the judicial software (automated fingerprint identification system (AFIS)) in order to successfully identify offenders remains to be researched. Most fingerprint recognition systems, such as the automated fingerprint identification system (AFIS), currently use level 1 and level 2 features. For level 3 features, a correspondingly high resolution of at least 1000 dpi is required. However, studies show that the inclusion of level 3 features can also lead to a better recognition rate. With 20 µm spatial scan resolution, a system has been reported to reach 1270 dpi and can, therefore, be used to identify level 3 features.[13–15]

Using the absorption-height correlation, it is possible to create a 3D model of the fingerprint. However, our model created using adeps lanae presents deviations in the model calculations compared to the literature. Thus, the created 3D model cannot be used to obtain concrete information about the actual layer thickness. However, it does provide information about the relative height distribution within the finger-

print. To determine absolute values, further studies must be done, in particular, height measurement of the applied fingerprints, as a ground truth for calculating the height model is necessary to create a suitable calculation model. The inaccuracy would then only lie in the concentration differences within the fingerprint itself. Then a calculation model that converts fast MIR scans into 3D data for high-resolution level 3 feature identification in very short acquisition times can be provided.

In summary, the built System quickens and optimizes the whole fingerprint acquisition process using infrared spectra. It can also open up the possibility of visualizing fingerprints that cannot be visualized using conventional non-invasive methods. In addition, it can be used prior to sample modification methods (chemical or physical) to provide additional assurance of identification.

Author contributions

Björn van Marwick: conceptualization, methodology, validation, investigation, visualization, resources, writing – original draft and writing – review & editing; Tim Kümmel: methodology, project administration, investigation, and software; Felix Lauer: investigation, resources and visualization; Felix Wühler: software, data curation, visualization and formal analysis; Jan Hoffmann: resources and supervision; Matthias Rädle: conceptualization, funding acquisition and supervision.

Conflicts of interest

The fingerprints presented in the study are made and shown with the consent of all other authors.

There are no further conflicts to declare.

Acknowledgements

This work was supported by the German Federal Ministry for Economic Affairs and Climate Action (BMWK), through the German Federation of Industrial Research Associations (AiF Project GmbH; Grant No: ZF4168604TS8, ZF4560205TS8 to M. R) and by Deutsche Forschungsgemeinschaft (DFG; Grant No: 410981386 to C.H).

The authors would like to thank Karl–Völker–Stiftung (KVS) at Mannheim University of Applied Sciences for financial support.

The article processing charge was funded by the Baden-Württemberg Ministry of Science, Research and Arts and the CeMOS Research and Transfer Center in the funding program Open Access Publishing. CeMOS also provided rooms, knowledge and united the authors.

Further the authors would like to thank Deborah Herdt for discussing approaches of the paper and sample preparation itself.

References

1 K. N. Win, K. Li, J. Chen, P. F. Viger and K. Li, Fingerprint classification and identification algorithms for criminal investigation: A survey, *Future Gener. Comput. Syst*, 2020, **110**, 758–771.
2 2012 proceedings of the 20th European Signal Processing Conference (EUSIPCO 2012). Bucharest, Romania, 27–31 August 2012, IEEE, Piscataway, NJ, 2012.
3 A. Dey, M. Tharmavaram, G. Pandey, D. Rawtani and C. Mustansar Hussain, Conventional and Emerging Biometrics Techniques in Forensic Investigations, in *Technology in Forensic Science: Sampling, Analysis, Data and Regulations*, ed. D. Rawtani and C. Mustansar Hussain, WILEY-VCH GmbH, Boschstr., 2020, ch. 9, pp. 175–197.
4 A. Piva, An Overview on Image Forensics, *ISRN Signal Process.*, 2013, **2013**, 1–22.
5 B. Herrmann and K.-S. Saternus, *Biologische Spurenkunde*, Springer, Berlin, Heidelberg, New York, 2007.
6 A. K. Jain, S. S. Arora, K. Cao, L. Best-Rowden and A. Bhatnagar, Fingerprint Recognition of Young Children, *IEEE Trans. Inf. Foren. Sec.*, 2017, **12**, 1501–1514.
7 E. Gutiérrez-Redomero, C. Alonso-Rodríguez, L. E. Hernández-Hurtado and J. L. Rodríguez-Villalba, Distribution of the minutiae in the fingerprints of a sample of the Spanish population, *Forensic Sci. Int.*, 2011, **208**, 79–90.
8 D. Meuwly, in *Encyclopedia of Biometrics*, ed. S. Z. Li and A. Jain, Springer US, Boston, MA, 2009, pp. 528–535.
9 V. Rekha, S. Gurupriya, S. Gayadhri and S. Sowmya, in 2019 IEEE International Conference on System, Computation, Automation and Networking (ICSCAN), IEEE, 32019, pp. 1–5.
10 T.-Y. Jea and V. Govindaraju, A minutia-based partial fingerprint recognition system, *Pattern Recognit.*, 2005, **38**, 1672–1684.
11 M. M. Ali, V. H. Mahale, P. Yannawar and A. T. Gaikwad, in 2016 International Conference on Electrical, Electronics, and Optimization Techniques (ICEEOT), IEEE, 32016, pp. 1334–1338.
12 F. Alonso-Fernandez, J. Bigun, J. Fierrez, H. Fronthaler, K. Kollreider and J. Ortega-Garcia, in *Guide to Biometric Reference Systems and Performance Evaluation*, ed. D. Petrovska-Delacrétaz, B. Dorizzi and G. Chollet, Springer London, London, 2009, pp. 51–88.
13 D. R. Ashbaugh, Quantitative-Qualitative Friction Ridge Analysis. In *An introduction to basic and advanced ridgeology*, CRC Press, [S.l.], 2021.
14 D. Maltoni, *Handbook of fingerprint recognition*, Springer, Berlin, 2nd edn, 2009.
15 A. Jain, Y. Chen and M. Demirkus, in 18th International Conference on Pattern Recognition (ICPR'06), IEEE, 2006, pp. 477–480.
16 *Technology in Forensic Science*, ed. D. Rawtani and C. M. Hussain, Wiley, 2020.
17 S. Madkour, S. Abeer, F. B. El Dine, Y. Elwakeel and N. AbdAllah, Development of latent fingerprints on non-

porous surfaces recovered from fresh and sea water, *Egypt. J. Forensic Sci.*, 2017, **7**, 3.
18 S. A. Sari, U. Qalbiah and I. C. Putri, Comparison between Latent Fingerprint Identification using Black Powder and Cyanoacrylate Glue, *Asian J. Chem.*, 2018, **30**, 2615–2620.
19 R. Yang and J. Lian, Studies on the development of latent fingerprints by the method of solid-medium ninhydrin, *Forensic Sci. Int.*, 2014, **242**, 123–126.
20 L. Schwarz and I. Klenke, Enhancement of ninhydrin- or DFO-treated latent fingerprints on thermal paper, *J. Forensic Sci.*, 2007, **52**, 649–655.
21 O. P. Jasuja, M. A. Toofany, G. Singh and G. S. Sodhi, Dynamics of latent fingerprints: the effect of physical factors on quality of ninhydrin developed prints–a preliminary study, *Sci. Justice*, 2009, **49**, 8–11.
22 D. A. Crown, The Development of Latent Fingerprints with Ninhydrin, *J. Crim. Law, Criminol. Police Sci.*, 1969, **60**, 258.
23 T. Nikkari, Comparative chemistry of sebum, *J. Invest. Dermatol.*, 1974, **62**, 257–267.
24 G. M. Mong, C. E. Petersen and T. R. Clauss, *Advanced Fingerprint Analysis Project Fingerprint Constituents*, 1999.
25 L. Liu, J. Wang, X. Wang, H. Wang, M. Li, T. Wu, G. Gao, X. Zheng, G. Liu, L. Fan, W. Shen, G. Ru, Z. Zhao and B. Z. Tang, High–Resolution Imaging of Latent Fingerprints through Near–Infrared Organoboron AIEgens, *Chin. J. Chem.*, 2023, **41**, 1465–1470.
26 L. Duan, Q. Zheng and T. Tu, Instantaneous High-Resolution Visual Imaging of Latent Fingerprints in Water Using Color-Tunable AIE Pincer Complexes, *Adv. Mater.*, 2022, **34**, e2202540.
27 M. Tahtouh, P. Despland, R. Shimmon, J. R. Kalman and B. J. Reedy, The application of infrared chemical imaging to the detection and enhancement of latent fingerprints: method optimization and further findings, *J. Forensic Sci.*, 2007, **52**, 1089–1096.
28 N. J. Crane, E. G. Bartick, R. S. Perlman and S. Huffman, Infrared spectroscopic imaging for noninvasive detection of latent fingerprints, *J. Forensic Sci.*, 2007, **52**, 48–53.
29 T. Chen, Z. D. Schultz and I. W. Levin, Infrared spectroscopic imaging of latent fingerprints and associated forensic evidence, *Analyst*, 2009, **134**, 1902–1904.
30 P. Hazarika, S. M. Jickells, K. Wolff and D. A. Russell, Imaging of latent fingerprints through the detection of drugs and metabolites, *Angew. Chem., Int. Ed.*, 2008, **47**, 10167–10170.
31 Y.-H. Chen, S.-Y. Kuo, W.-K. Tsai, C.-S. Ke, C.-H. Liao, C.-P. Chen, Y.-T. Wang, H.-W. Chen and Y.-H. Chan, Dual Colorimetric and Fluorescent Imaging of Latent Fingerprints on Both Porous and Nonporous Surfaces with Near-Infrared Fluorescent Semiconducting Polymer Dots, *Anal. Chem.*, 2016, **88**, 11616–11623.
32 R. S. Croxton, M. G. Baron, D. Butler, T. Kent and V. G. Sears, Variation in amino acid and lipid composition of latent fingerprints, *Forensic Sci. Int.*, 2010, **199**, 93–102.
33 B. Hartzell-Baguley, R. E. Hipp, N. R. Morgan and S. L. Morgan, Chemical Composition of Latent Fingerprints by Gas Chromatography–Mass Spectrometry. An Experiment for an Instrumental Analysis Course, *J. Chem. Educ.*, 2007, **84**, 689.
34 C. Weyermann, C. Roux and C. Champod, Initial results on the composition of fingerprints and its evolution as a function of time by GC/MS analysis, *J. Forensic Sci.*, 2011, **56**, 102–108.
35 L. Fan, Y. Jia, L. Cui, X. Li and C. He, Analysis of sensitive skin barrier function: basic indicators and sebum composition, *Int. J. Cosmet. Sci.*, 2018, **40**, 117–126.
36 K. Sato and F. Sato, Individual variations in structure and function of human eccrine sweat gland, *Am. J. Physiol.*, 1983, **245**, R203–R208.
37 K. Sato, R. Leidal and F. Sato, Morphology and development of an apoeccrine sweat gland in human axillae, *Am. J. Physiol.*, 1987, **252**, R166–R180.
38 T. Verde, R. J. Shephard, P. Corey and R. Moore, Sweat composition in exercise and in heat, *J. Appl. Physiol.: Respir., Environ. Exercise Physiol.*, 1982, **53**, 1540–1545.
39 Y.-L. Chen, W.-H. Kuan and C.-L. Liu, Comparative Study of the Composition of Sweat from Eccrine and Apocrine Sweat Glands during Exercise and in Heat, *Int. J. Environ. Res. Public Health*, 2020, **17**, 3377.
40 L. B. Baker and A. S. Wolfe, Physiological mechanisms determining eccrine sweat composition, *Eur. J. Appl. Physiol.*, 2020, **120**, 719–752.
41 C.-Y. Cui and D. Schlessinger, Eccrine sweat gland development and sweat secretion, *Exp. Dermatol.*, 2015, **24**, 644–650.
42 K. Wilke, A. Martin, L. Terstegen and S. S. Biel, A short history of sweat gland biology, *Int. J. Cosmet. Sci.*, 2007, **29**, 169–179.
43 S. Robinson and A. H. Robinson, Chemical composition of sweat, *Physiol. Rev.*, 1954, **34**, 202–220.
44 L. B. Baker, Physiology of sweat gland function: The roles of sweating and sweat composition in human health, *Temperature*, 2019, **6**, 211–259.
45 K. Sato and F. Sato, Sweat secretion by human axillary apoeccrine sweat gland in vitro, *Am. J. Physiol.*, 1987, **252**, R181–R187.
46 S. S. Bala and P. N. Ghosh, Fermi resonance, hydrogen bonding and hot bands in the IR spectra of thiourea and urea, *J. Mol. Struct.*, 1983, **101**, 69–77.
47 J. B. Peri, Infrared Study of Adsorption of Ammonia on Dry γ-Alumina 1, *J. Phys. Chem.*, 1965, **69**, 231–239.
48 C. Petibois, A. M. Melin, A. Perromat, G. Cazorla and G. Déléris, Glucose and lactate concentration determination on single microsamples by Fourier-transform infrared spectroscopy, *J. Lab. Clin. Med.*, 2000, **135**, 210–215.
49 J. M. Cardamone, Investigating the microstructure of keratin extracted from wool: Peptide sequence (MALDI-TOF/TOF) and protein conformation (FTIR), *J. Mol. Struct.*, 2010, **969**, 97–105.
50 M. V. Korolevich, R. G. Zhbankov and V. V. Sivchik, Calculation of absorption band frequencies and intensi-

ties in the IR spectrum of α-d-glucose in a cluster, *J. Mol. Struct.*, 1990, **220**, 301–313.
51 L. M. Miller, M. W. Bourassa and R. J. Smith, FTIR spectroscopic imaging of protein aggregation in living cells, *Biochim. Biophys. Acta*, 2013, **1828**, 2339–2346.
52 C. S. Marvel and J. R. Elliott, The structure of urea-formaldehyde resins, *J. Am. Chem. Soc.*, 1946, **68**, 1681–1686.
53 D. Huster, A. Vogel, C. Katzka, H. A. Scheidt, H. Binder, S. Dante, T. Gutberlet, O. Zschörnig, H. Waldmann and K. Arnold, Membrane insertion of a lipidated ras peptide studied by FTIR, solid-state NMR, and neutron diffraction spectroscopy, *J. Am. Chem. Soc.*, 2003, **125**, 4070–4079.
54 B. Brauer, M. Pincu, V. Buch, I. Bar, J. P. Simons and R. B. Gerber, Vibrational spectra of α-glucose, β-glucose, and sucrose: anharmonic calculations and experiment, *J. Phys. Chem. A*, 2011, **115**, 5859–5872.
55 G. Cassanas, M. Morssli, E. Fabrègue and L. Bardet, Vibrational spectra of lactic acid and lactates, *J. Raman Spectrosc.*, 1991, **22**, 409–413.
56 N. W. Cant and L. H. Little, An infrared study of the adsorption of ammonia on porous vycor glass, *Can. J. Chem.*, 1964, **42**, 802–809.
57 R. Keuleers, H. O. Desseyn, B. Rousseau and C. van Alsenoy, Vibrational Analysis of Urea, *J. Phys. Chem. A*, 1999, **103**, 4621–4630.
58 A. A. Tsyganenko, D. V. Pozdnyakov and V. N. Filimonov, Infrared study of surface species arising from ammonia adsorption on oxide surfaces, *J. Mol. Struct.*, 1975, **29**, 299–318.
59 R. M. B. Mackenna, V. R. Wheatley and A. Wormall, The composition of the surface skin fat ('sebum') from the human forearm, *J. Invest. Dermatol.*, 1950, **15**, 33–47.
60 M. Picardo, M. Ottaviani, E. Camera and A. Mastrofrancesco, Sebaceous gland lipids, *Derm.-Endocrinol.*, 2009, **1**, 68–71.
61 D. Downfng and J. S. Strauss, Synthesis and composition of surface lipids of human skin, **https://core.ac.uk/download/pdf/82302545.pdf**, (accessed 5 October 2021).
62 S. C. Green, M. E. Stewart and D. T. Downing, Variation in sebum fatty acid composition among adult humans, *J. Invest. Dermatol.*, 1984, **83**, 114–117.
63 V. R. Wheatley and A. T. James, Studies of sebum. 7. The composition of the sebum of some common rodents, *Biochem. J.*, 1957, **65**, 36–42.
64 E. W. Powell and G. W. Beveridge, Sebum excretion and sebum composition in adolescent men with and without acne vulgaris, *Br. J. Dermatol.*, 1970, **82**, 243–249.
65 B. Boughton and V. R. Wheatley, The Fatty Acid Composition of the Skin Surface Fat ('Sebum") of Normal Human Subjects11From the Departments of Biochemistry and Dermatology, Medical College of St. Bartholomew's Hospital, London, E.C.1, *J. Invest. Dermatol.*, 1959, **33**, 49–55.
66 S. S. Shetage, M. J. Traynor, M. B. Brown, M. Raji, D. Graham-Kalio and R. P. Chilcott, Effect of ethnicity, gender and age on the amount and composition of residual skin surface components derived from sebum, sweat and epidermal lipids, *Sking Res. Technol.*, 2014, **20**, 97–107.
67 R. R. Wickett and M. O. Visscher, Structure and function of the epidermal barrier, *Am. J. Infect. Control*, 2006, **34**, S98–S110.
68 P. M. Elias, J. Goerke and D. S. Friend, Mammalian epidermal barrier layer lipids: composition and influence on structure, *J. Invest. Dermatol.*, 1977, **69**, 535–546.
69 H. L. Barros and V. Stefani, A new methodology for the visualization of latent fingermarks on the sticky side of adhesive tapes using novel fluorescent dyes, *Forensic Sci. Int.*, 2016, **263**, 83–91.
70 G. S. Sodhi and J. Kaur, Physical developer method for detection of latent fingerprints: A review, *Egypt. J. Forensic Sci.*, 2016, **6**, 44–47.
71 E. Brunelle, C. Huynh, A. M. Le, L. Halámková, J. Agudelo and J. Halámek, New Horizons for Ninhydrin: Colorimetric Determination of Gender from Fingerprints, *Anal. Chem.*, 2016, **88**, 2413–2420.
72 M. M. Schulz, H.-D. Wehner, W. Reichert and M. Graw, Ninhydrin-dyed latent fingerprints as a DNA source in a murder case, *J. Clin. Forensic Med.*, 2004, **11**, 202–204.
73 R. Rohatgi, G. S. Sodhi and A. K. Kapoor, Small particle reagent based on crystal violet dye for developing latent fingerprints on non-porous wet surfaces, *Egypt. J. Forensic Sci.*, 2015, **5**, 162–165.
74 O. P. Jasuja, G. D. Singh and G. S. Sodhi, Development of Latent Fingerprints on the Sticky Side of Adhesive Tapes: Phase Transfer Catalyst-Based Formulation, *Can. Soc. Forensic Sci. J.*, 2007, **40**, 1–13.
75 M. Stoilovic, Improved method for DFO development of latent fingerprints, *Forensic Sci. Int.*, 1993, **60**, 141–153.
76 R. Cook, N. Mitchell and J. Henry, Assessment of Diamond™ Nucleic Acid Dye for the identification and targeted sampling of latent DNA in operational casework, *Forensic Sci. Int.: Genet.*, 2021, **55**, 102579.
77 Y. Gülekçi, Effects of Environmental Factors on Fingerprint Development, *Eur. J. Sci. Technol.*, 2022, **32**, 463–470.
78 P. Chingthongkham, S. Chomean, P. Suppajariyawat and C. Kaset, Enhancement of bloody fingerprints on non-porous surfaces using Lac dye (Laccifer lacca), *Forensic Sci. Int.*, 2020, **307**, 110119.
79 Y. Harush-Brosh, Y. Levy-Herman, R. Bengiat, C. Oz, M. Levin-Elad, M. Horowitz and M. Faerman, Back to Amido Black: Uncovering touch DNA in blood-contaminated fingermarks, *J. Forensic Sci.*, 2021, **66**, 1697–1703.
80 V. Prasad, L. Prasad, S. Lukose and P. Agarwal, Latent fingerprint development by using silver nanoparticles and silver nitrate-A comparative study, *J. Forensic Sci.*, 2021, **66**, 1065–1074.
81 A. Oleszko, J. Hartwich, A. Wójtowicz, M. Gąsior-Głogowska, H. Huras and M. Komorowska, Comparison of FTIR-ATR and Raman spectroscopy in determination of

VLDL triglycerides in blood serum with PLS regression, *Spectrochim. Acta, Part A*, 2017, **183**, 239–246.
82 D. W. Hall, S. N. Marshall, K. C. Gordon and D. P. Killeen, Rapid Quantitative Determination of Squalene in Shark Liver Oils by Raman and IR Spectroscopy, *Lipids*, 2016, **51**, 139–147.
83 H.-U. Gremlich, in *Handbook of Analytical Techniques*, ed. H. Gnzler and A. Williams, Wiley-VCH Verlag GmbH, Weinheim, Germany, 2001, pp. 465–507.
84 K. M. Antoine, S. Mortazavi, A. D. Miller and L. M. Miller, Chemical differences are observed in children's versus adults' latent fingerprints as a function of time, *J. Forensic Sci.*, 2010, **55**, 513–518.
85 M. A. de Souza, A. Santos, S. W. Da Silva, J. W. Braga and M. H. Sousa, Diffuse Reflectance FTIR of Latent Fingerprints and Discriminant Analysis for Sex Identification in Humans, *J. Braz. Chem. Soc.*, 2023, 820–824.
86 Y. P. Zhang, R. N. Lewis, R. S. Hodges and R. N. McElhaney, FTIR spectroscopic studies of the conformation and amide hydrogen exchange of a peptide model of the hydrophobic transmembrane alpha-helices of membrane proteins, *Biochemistry*, 1992, **31**, 11572–11578.
87 G. Kwak, W.-E. Lee, W.-H. Kim and H. Lee, Fluorescence imaging of latent fingerprints on conjugated polymer films with large fractional free volume, *Chem. Commun.*, 2009, 2112–2114.
88 D. Peng, S. He, Y. Zhang, L. Yao, W. Nie, Z. Liao, W. Cai and X. Ye, Blue light-induced rare-earth free phosphors for the highly sensitive and selective imaging of latent fingerprints based on enhanced hydrophobic interaction, *J. Materiomics*, 2022, **8**, 229–238.
89 R. M. Connatser, S. M. Prokes, O. J. Glembocki, R. L. Schuler, C. W. Gardner, S. A. Lewis and L. A. Lewis, Toward surface-enhanced Raman imaging of latent fingerprints, *J. Forensic Sci.*, 2010, **55**, 1462–1470.
90 L. Zhao, X. Huang and W. Hu, Interfacial Separation-Enabled All-Dry Approach for Simultaneous Visualization, Transfer, and Enhanced Raman Analysis of Latent Fingerprints, *ACS Appl. Mater. Interfaces*, 2017, **9**, 37350–37356.
91 B. Figueroa, Y. Chen, K. Berry, A. Francis and D. Fu, Label-Free Chemical Imaging of Latent Fingerprints with Stimulated Raman Scattering Microscopy, *Anal. Chem.*, 2017, **89**, 4468–4473.
92 E. Widjaja, Latent fingerprints analysis using tape-lift, Raman microscopy, and multivariate data analysis methods, *Analyst*, 2009, **134**, 769–775.
93 A. Skriba and V. Havlicek, Mass spectrometry imaging of illicit drugs in latent fingerprints by matrix-free and matrix-assisted desorption/ionization techniques, *Eur. J. Mass Spectrom.*, 2018, **24**, 124–128.
94 H. Chen, R. Ma and M. Zhang, Recent Progress in Visualization and Analysis of Fingerprint Level 3 Features, *ChemistryOpen*, 2022, **11**, e202200091.
95 J. A. Bailey and J. S. Crane, Use of nitrogen cryogun for separating duct tape and recovery of latent fingerprints with a powder suspension method, *Forensic Sci. Int.*, 2011, **210**, 170–173.
96 S.-M. Kim and S. Hong, A Comparison of Adhesive Tape-Separation Methods from Surfaces; Dipping in Liquid Nitrogen, Liquid Nitrogen Spray and an Adhesive Neutralizer Method, *J. Forensic. Res.*, 2016, **07**, 1000346.
97 B. G. Stephens, G. Nazareno, M. Block and P. Hnatow, Use of liquid nitrogen to remove duct tape from a homicide victim, *Am. J. Forensic Med. Pathol.*, 1999, **20**, 154–157.
98 D. F. Swinehart, The Beer-Lambert Law, *J. Chem. Educ.*, 1962, **39**, 333.
99 H. Günzler and H.-U. Gremlich, IR-Spectroskopie, in *Eine Einführung*, Wiley-VCH, Weinheim, 4th edn, 2003.
100 2019 IEEE International Conference on System, Computation, Automation and Networking (ICSCAN), IEEE, 32019.
101 I. V. Hertel and C.-P. Schulz, *Atome, Moleküle und optische Physik 1*, Springer Berlin Heidelberg, Berlin, Heidelberg, 2017.
102 J. Haus, Optical sensors. In *Basics and applications*, Wiley-VCH, Weinheim, 2010.
103 W. Gottwald and G. Wachter, *IR-Spektroskopie für Anwender*, Wiley-VCH, Weinheim, 1997.
104 T. Hecht, *Physikalische Grundlagen der IR-Spektroskopie*, in *Von Mechanischen Schwingungen Zur Vorhersage und Interpretation Von IR-Spektren*, Spektrum Akademischer Verlag GmbH, Wiesbaden, 2019.
105 L. J. Bellamy, *The Infra-red Spectra of Complex Molecules*, Springer Netherlands, Dordrecht, 1975.
106 K. Fernandez and E. Agosin, Quantitative analysis of red wine tannins using Fourier-transform mid-infrared spectrometry, *J. Agric. Food Chem.*, 2007, **55**, 7294–7300.
107 R. Linder, K. Seefeld, A. Vavra and K. Kleinermanns, Gas phase infrared spectra of nonaromatic amino acids, *Chem. Phys. Lett.*, 2008, **453**, 1–6.
108 S. Low-Ying, R. Shaw, M. Leroux and H. H. Mantsch, Quantitation of glucose and urea in whole blood by mid-infrared spectroscopy of dry films, *Vib. Spectrosc.*, 2002, **28**, 111–116.
109 *OCM 2019 - Optical Characterization of Materials: Conference Proceedings*, ed. J. Beyerer, F. Puente León and T. Längle, KIT Scientific Publishing, 2019.
110 T. Kümmel, T. Teumer, P. Dörnhofer, F.-J. Methner, B. Wängler and M. Rädle, Contrast enhancement of surface layers with fast middle-infrared scanning, *Heliyon*, 2019, **5**, e02442.
111 T. Kümmel, B. van Marwick, M. Rittel, C. Ramallo Guevara, F. Wühler, T. Teumer, B. Wängler, C. Hopf and M. Rädle, Rapid brain structure and tumour margin detection on whole frozen tissue sections by fast multi-photometric mid-infrared scanning, *Sci. Rep.*, 2021, **11**, 11307.
112 Z. Ashraf, U. Pasha, V. Greenstone, J. Akbar, E. Apenbrinck, G. N. Foulks and D. Borchman,

Quantification of human sebum on skin and human meibum on the eye lid margin using Sebutape®, spectroscopy and chemical analysis, *Curr. Eye Res.*, 2011, **36**, 553–562.

113 L. Brancaleon, M. P. Bamberg and N. Kollias, Spectral Differences between Stratum Corneum and Sebaceous Molecular Components in the Mid-IR, *Appl. Spectrosc.*, 2000, **54**, 1175–1182.

114 R. M. El-Abassy, P. Donfack and A. Materny, Rapid Determination of Free Fatty Acid in Extra Virgin Olive Oil by Raman Spectroscopy and Multivariate Analysis, *J. Am. Oil Chem. Soc.*, 2009, **86**, 507–511.

115 G. Sansone and J. G. Hamilton, Glyceryl ether, wax ester and triglyceride composition of the mouse preputial gland, *Lipids*, 1969, **4**, 435–440.

116 K.-Z. Liu, R. A. Shaw, A. Man, T. C. Dembinski and H. H. Mantsch, Reagent-free, simultaneous determination of serum cholesterol in HDL and LDL by infrared spectroscopy, *Clin. Chem.*, 2002, **48**, 499–506.

117 D. Fu, C. Leng, J. Kelley, G. Zeng, Y. Zhang and Y. Liu, ATR-IR study of ozone initiated heterogeneous oxidation of squalene in an indoor environment, *Environ. Sci. Technol.*, 2013, **47**, 10611–10618.

118 G. S. Gooris and J. A. Bouwstra, Infrared spectroscopic study of stratum corneum model membranes prepared from human ceramides, cholesterol, and fatty acids, *Biophys. J.*, 2007, **92**, 2785–2795.

119 A. A. Christy and P. K. Egeberg, Quantitative determination of saturated and unsaturated fatty acids in edible oils by infrared spectroscopy and chemometrics, *Chemom. Intell. Lab. Syst.*, 2006, **82**, 130–136.

120 T. Eren and S. H. Küsefoğlu, Hydroxymethylation and polymerization of plant oil triglycerides, *J. Appl. Polym. Sci.*, 2004, **91**, 4037–4046.

121 W. Mäntele and E. Deniz, UV-VIS absorption spectroscopy: Lambert-Beer reloaded, *Spectrochim. Acta, Part A*, 2017, **173**, 965–968.

122 A. Larena, G. Pinto and F. Millán, Using the Lambert-Beer law for thickness evaluation of photoconductor coatings for recording holograms, *Appl. Surf. Sci.*, 1995, **84**, 407–411.

123 M. Ludvigsson, J. Lindgren and J. Tegenfeldt, FTIR study of water in cast Nafion films, *Electrochim. Acta*, 2000, **45**, 2267–2271.

124 A. Vasylieva, I. Doroshenko, Y. Vaskivskyi, Y. Chernolevska and V. Pogorelov, FTIR study of condensed water structure, *J. Mol. Struct.*, 2018, **1167**, 232–238.

125 T. P. Abbott, H. Nabetani, D. J. Sessa, W. J. Wolf, M. N. Liebman and R. K. Dukor, Effects of Bound Water on FTIR Spectra of Glycinin, *J. Agric. Food Chem.*, 1996, **44**, 2220–2224.

126 A. Fadlelmoula, D. Pinho, V. H. Carvalho, S. O. Catarino and G. Minas, Fourier Transform Infrared (FTIR) Spectroscopy to Analyse Human Blood over the Last 20 Years: A Review towards Lab-on-a-Chip Devices, *Micromachines*, 2022, **13**, 187.

127 V. E. Sitnikova, M. A. Kotkova, T. N. Nosenko, T. N. Kotkova, D. M. Martynova and M. V. Uspenskaya, Breast cancer detection by ATR-FTIR spectroscopy of blood serum and multivariate data-analysis, *Talanta*, 2020, **214**, 120857.

128 D. Muscat, M. J. Tobin, Q. Guo and B. Adhikari, Understanding the distribution of natural wax in starch-wax films using synchrotron-based FTIR (S-FTIR), *Carbohydr. Polym.*, 2014, **102**, 125–135.

129 A. Bucio, R. Moreno-Tovar, L. Bucio, J. Espinosa-Dávila and F. Anguebes-Franceschi, Characterization of Beeswax, Candelilla Wax and Paraffin Wax for Coating Cheeses, *Coatings*, 2021, **11**, 261.

130 P. Dawson and A. M. Goodwill, A Review of Weapon Choice in Violent and Sexual Crime, *BLR*, 2013, **04**, 20–27.

131 M. E. Hunter and C. C. Love, Types of weapons and patterns of use in a forensic hospital, *Hosp. Community Psych.*, 1993, **44**, 1082–1085.

132 W. W. Coblentz, The reflecting power of various metals, *J. Franklin Inst.*, 1910, **170**, 169–193.

133 M. Fabian, E. Lewis, T. Newe and S. Lochmann, Optical fibre cavity for ring-down experiments with low coupling losses, *Meas. Sci. Technol.*, 2010, **21**, 94034.

134 J. de Alcaraz-Fossoul, M. Mancenido, E. Soignard and N. Silverman, Application of 3D Imaging Technology to Latent Fingermark Aging Studies, *J. Forensic Sci.*, 2019, **64**, 570–576.

135 Advanced studies in biometrics. Summer School on Biometrics, Alghero, Italy, June 2–6, 2003: revised selected lectures and papers.

136 R. M. Brown and A. R. Hillman, Electrochromic enhancement of latent fingerprints by poly(3,4-ethylenedioxythiophene), *Phys. Chem. Chem. Phys.*, 2012, **14**, 8653–8661.

137 G. L. Thomas, The physics of fingerprints and their detection, *J. Phys. E: Sci. Instrum.*, 1978, **11**, 722–731.